Push-pull regulation of exploratory behavior by two opposing hippocampal to prefrontal cortex pathways

Candela Sánchez-Bellot [1] and Andrew F. MacAskill [1*]
[1]Department of Neuroscience, Physiology and Pharmacology, University College London, Gower St, London, WC1E 6BT.
*Corresponding author: a.macaskill@ucl.ac.uk

We found that the hippocampal projection to prefrontal cortex is composed of two parallel circuits located in the superficial or deep hippocampal pyramidal layers. These circuits have unique upstream and downstream connectivity, and are differentially active during exploration of a potentially threatening environment. Artificial activation of the superficial circuit promotes exploration via preferential recruitment of PFC inhibition, while activation of the deep circuit promotes avoidance via direct excitation.

The decision to explore a novel, potentially threatening environment is essential for survival. Too little exploration reduces the likelihood of finding novel sources of reward, while too much increases risk such as injury. Excitatory input into the prefrontal cortex (PFC) arising from neurons in the CA1/subiculum border of the ventral hippocampus (vH) is crucial for the decision to explore potentially threatening locations[1-5]. Activation of PFC circuitry drives avoidance, while inactivation promotes exploration. Consistent with its controlling role, vH is able to both activate and inhibit PFC circuitry dependent on task demands[6-8]. This apparent dichotomy of function is thought to arise through flexible recruitment of both excitatory and local inhibitory circuitry[1,9-12]. However, little is known about the synaptic and circuit mechanisms that might underlie this dual role. Notably, pyramidal neurons in vH are comprised of a series of segregated populations that have unique genetics, physiology and circuit function[13]. Therefore, we hypothesized that the apparent dual role of vH input in PFC may be a result of the projection being composed of more than one population of neurons, each recruited at different points during behavior, with distinct downstream connectivity within PFC.

To investigate this possibility, we first labelled neurons that project to the PFC with an injection of the retrograde tracer cholera toxin (CTXβ, ***Fig.1a***). Strikingly, labelled neurons in vH consistently formed two distinct layers at the extreme poles of the radial axis (***Fig.1b, Sup.Fig.1***) – one along the most superficial layer and one in the deep layer – corresponding to layer II and IV of subiculum[14]. This layered organization was unique to PFC-projecting neurons and was not found in projections to other downstream regions (***Sup.Fig.1***).

We hypothesized that these two spatially distinct populations may represent two circuits that could underlie the dual role of the vH to PFC (vH-PFC) projection. Consistent with this idea, the two populations had distinct morphological and electrophysiological properties (***Sup.Fig.2***), reminiscent of dorsally located superficial and deep neurons[15]. Similarly, RNA sequencing revealed multiple genes that were differentially expressed across the two populations (***Sup.Fig.3***) including *Calbindin1* (*Calb1*) which was enriched in the superficial PFC-projecting population[16]. We confirmed selective *Calb1* expression in the superficial layer using fluorescent labelling with a retrograde 'switch' virus injected into PFC, where the identity of the fluorescent reporter in vH was dependent on the expression of *Calb1* (***Fig.1c,d***). Thus, hippocampal neurons that project to PFC can be split into two populations with distinct molecular, cellular and physiological properties, consistent with the hypothesis of a heterogeneous vH-PFC circuit.

We next tested if this parallel output organization was mirrored by unique afferent input. We first used *tracing the relationship between input and output* (TRIO) to show dense input onto vH-PFC neurons from CA3, entorhinal cortex (ENT), anterior thalamus (ATh), and the diagonal band of Broca (DBB, ***Sup.Fig.4***). Using channelrhodopsin assisted circuit mapping (CRACM) in acute slices of vH, we found that while CA3 terminal stimulation resulted in roughly equal excitatory synaptic drive in both superficial and deep neurons, ENT input was biased towards superficial layer neurons, and both DBB and ATh input was markedly biased

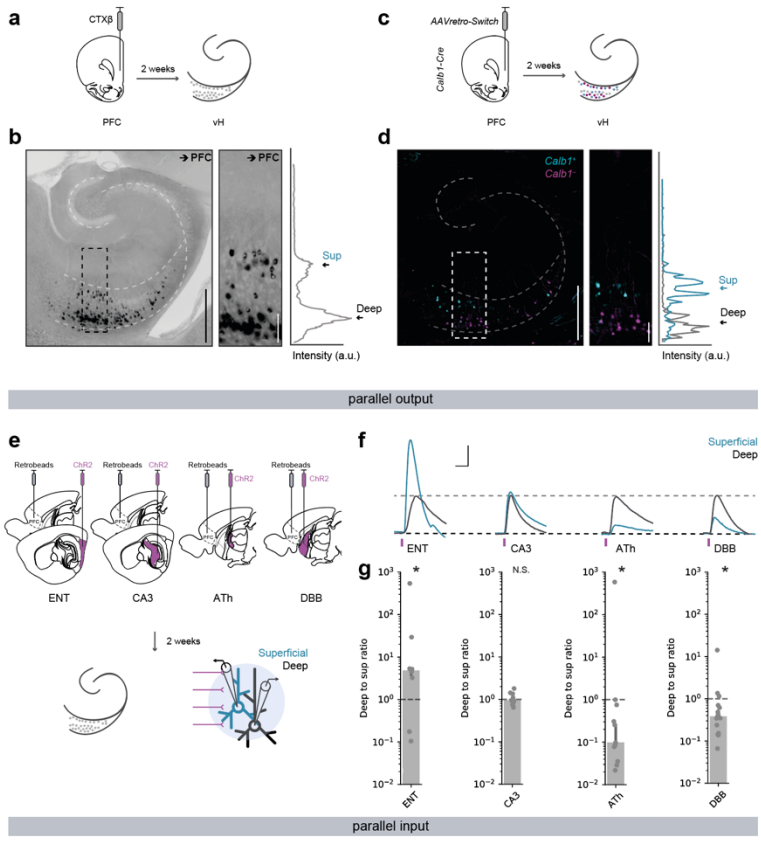

Figure 1 | Hippocampal neurons projecting to PFC form two populations segregated across the radial axis.

a) Schematic of cholera toxin (CTXβ) injection into PFC and retrograde labelling in hippocampus.

b) *Left,* Transverse slice of hippocampus labelled with CTXβ. *Right*, zoom of retrogradely labelled neurons in boxed region, with fluorescence intensity profile. Arrows highlight the two distinct peaks of fluorescence at the two extremes of the radial axis. See ***Sup.Fig.1*** for detailed quantification. Scale bar = 500 µm (*Left*) 100 µm (*Right*).

c) *AAVretro-Switch* injection into the PFC of *Calb1-Cre* mice and subsequent Cre-dependent retrograde labelling in hippocampus.

d) Transverse slice of hippocampus labelled with *AAVretro-Switch*. Cyan labels *Calb1*$^{+}$ PFC-projecting neurons and magenta labels *Calb1*$^{-}$ neurons. *Right*, zoom of retrogradely labelled neurons in boxed region, with fluorescence intensity profile for *Calb1*$^{+}$ (*cyan*) and *Calb1*$^{-}$ (*black*) neurons. Arrows highlight the two genetically distinct peaks of fluorescence at the two extremes of the radial axis. Scale bar = 500 µm (*Left*) 100 µm (*Right*).

e) Schematic showing experimental setup. ChR2 injected into each afferent region and retrobeads injected into PFC. 2 weeks later input-specific connectivity was assessed using paired recordings of superficial and deep vH-PFC neurons in acute slices.

f) Light-evoked responses in example pairs of superficial (*blue*) and deep (*black*) layer PFC-projecting hippocampal neurons in response to afferent input. Superficial responses are scaled to neighboring deep responses. Scale bar = 20 ms, 0.5 fold of deep neuron response. Purple tick represents the light stimulus.

g) Summary of the ratio of superficial : deep neuron EPSP for each afferent input. Higher values mean input is biased to superficial neurons, low values towards deep layer neurons. Note log scale. ENT input is biased towards activation of superficial neurons ($V = 44$, $p = 0.007$, $n = 9$ pairs, Wilcoxon), CA3 input is equivalent onto superficial and deep layer neurons ($V = 27$, $p = 1.0$, $n = 10$ pairs, Wilcoxon), ATh and DBB input is biased towards activation of deep neurons (ATh: $V = 12$, $p = 0.034$, $n = 7$ pairs; DBB: $V = 24$, $p = 0.041$, $n = 15$ pairs, Wilcoxon). Here and throughout data is presented as individual data points overlaid on the mean ± s.e.m.

towards deep-layer neurons (***Fig.1e-g, Sup.Fig.4***). Thus, hippocampal neurons that project to PFC can be split into two populations that receive distinct local- and long-range afferent input, suggesting they may route unique information to PFC.

Consistent with our hypothesis, these two populations of vH neurons are well placed to provide the distinct influence on PFC circuitry. Therefore, we next asked whether they have distinct synaptic connectivity within PFC. We had two hypotheses: first the two spatially segregated layers in vH may connect with distinct spatial locations within PFC. For example, inhibitory connectivity between prelimbic (PL) and infralimbic (IL) PFC is crucial for determining PFC output[17,18]. Alternatively, we thought these two populations may differentially connect to excitatory or inhibitory neurons within PFC, to directly alter local circuit balance[1,11].

We used a transgenic and viral approach (see methods) to label either superficial or deep layer neurons in vH (***Fig.2a-c***). We found that targeting of axons from the two layers throughout PFC was remarkably similar (***Fig.2d,e***). This was the case when we examined gross axon distribution across regions, where both populations targeted infralimbic (IL), prelimbic (PL) and medial orbital (ORBm) PFC to a similar extent (***Fig.2f***). This was also the case when we examined axon distribution across dorso-ventral, medio-lateral or raustro-caudal axes (***Sup.Fig.5***). Together, this precludes the two populations targeting unique topological domains of PFC.

In contrast, monosynaptic rabies tracing from either inhibitory interneurons (using *VGAT+ starter cells*) or excitatory neurons (using *CaMKii+ starter cells*) in PFC (***Fig.2g,h***) showed dramatic differences in the targeting of excitatory vs inhibitory neurons in PFC by each layer in vH. Both superficial and deep layer vH neurons targeted interneurons in PFC, however, input to pyramidal neurons was almost entirely derived from deep layer vH neurons. We confirmed this distinct targeting using CRACM of input from superficial or deep layer vH in recordings from layer V pyramidal neurons in acute slices of PFC. These recordings confirmed that the superficial layer of vH drives more feedforward inhibition in PFC compared to the deep layer, which drives more excitation (***Fig2j-l***).

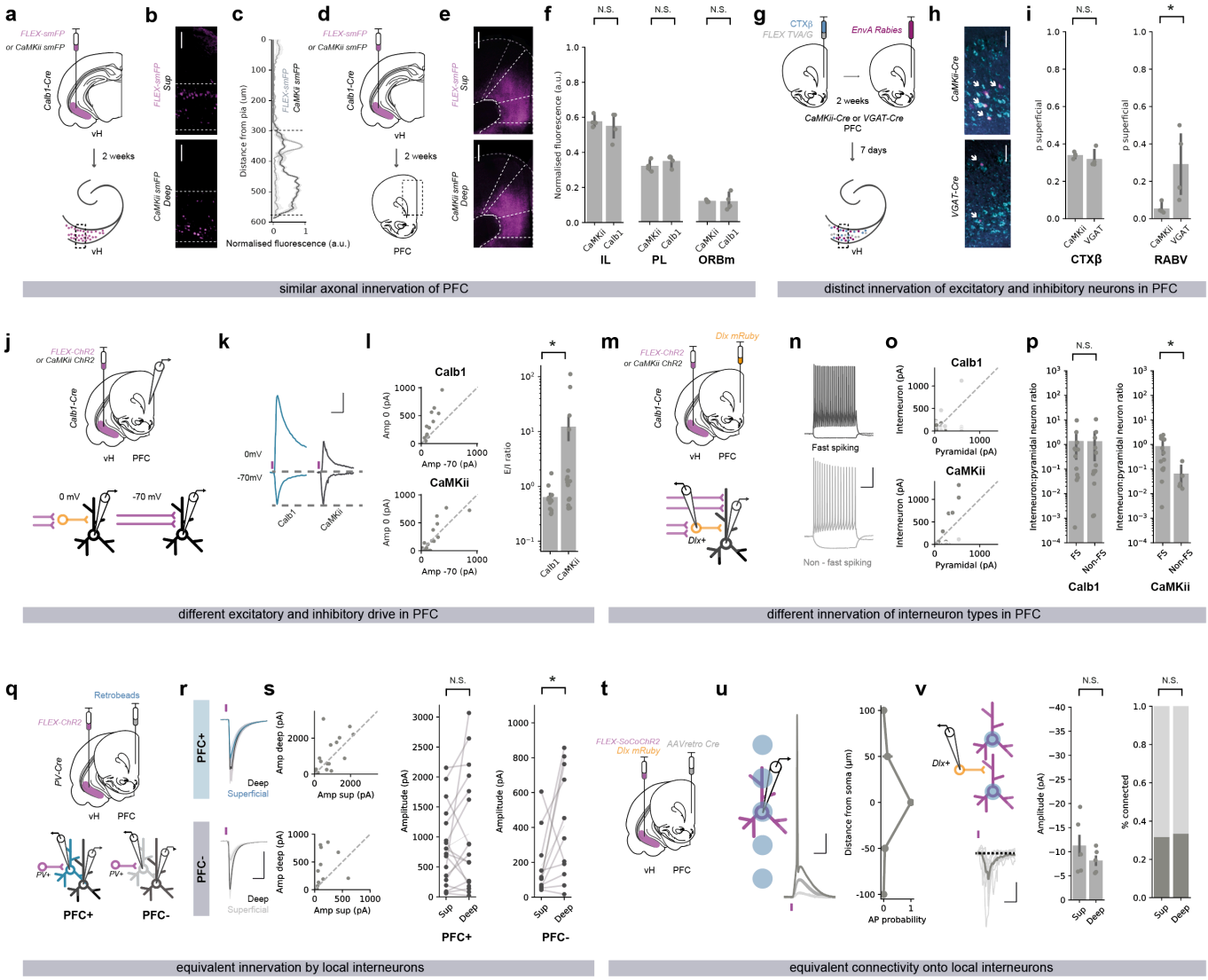

Figure 2 | Hippocampal input to PFC forms a long-range push pull circuit.

a-c) Strategy to express anterograde tracer (*smFP*) in each layer of vH in *Calb1-Cre* mice. **b**) Distribution of labelled cells in the two conditions – note preferential expression in superficial (*top*) and deep (*bottom*) layers. Scale bar = 100 µm, summary of n = 4 injections shown in (**c**).

d,e) Strategy to label axons from superficial and deep layers and example images of axons in PFC from each layer in vH. Scale bar = 100 µm.

f) Quantification of axon fluorescence intensity in IL, PL and ORBm regions of PFC. Note similar distribution of fluorescence, see also ***Sup.Fig.5***.

g) Strategy to label neurons projecting to inhibitory and excitatory neurons in PFC.

h) Transverse slice of hippocampus labelled with CTXβ (*cyan*) and rabies (*magenta*) after tracing from excitatory (*top*) or inhibitory (*bottom*) neurons in PFC. Note the restriction of rabies labelling from excitatory neurons to the deep layer. Scale bar = 100 µm.

i) Proportion of CTXβ positive neurons (*left*) and rabies positive neurons (*right*) in the superficial layer (see methods, and ***Sup.Fig.5***). Note equivalent distribution of CTXβ across both conditions (U = 4, p = 0.3, n = 4 injections per condition, Mann Whitney), but a marked absence of neurons projecting to excitatory PFC neurons in the superficial layer (U = 16, p = 0.03, n = 4 injections per condition, Mann Whitney).

j) Strategy to record E:I ratio in PFC from each layer in vH.

k,l) Responses to superficial (*blue*) or deep (*black*) hippocampal inputs at -70 mV (EPSCs) and 0 mV (IPSCs) in deep layer PFC neurons. Purple tick indicates light pulse. Scale bar = 20 ms and 0.5 (fold response amplitude at -70 mV, which is normalized to 1). Summarized in (**l**). Input from superficial neurons has a greater inhibitory contribution than that of deep neurons. (U = 51, p = 0.017, n = 12 (*Sup*), 18 (*Deep*), Mann Whitney).

m) Strategy to record input from the two layers of vH onto identified interneurons in PFC.

n) Example current clamp recordings from fast-spiking (FS - *black*) and non-fast-spiking (Non-FS - *grey*) neurons in PFC. For details of classification see ***Sup.Fig.6***. Scale bar = 30 mV, 100 ms.

o) Responses to superficial (*top*) and deep (*bottom*) hippocampal input at -70 mV (EPSCs) onto deep layer PFC neurons and neighboring FS (*black*) or non-FS interneurons (*grey*) summarized in (**p**). Input from superficial neurons innervates both FS and non-FS interneurons to the same extent (U = 84, p = 0.77, n = 12 pairs (FS), 13 pairs (non-FS), Mann Whitney), while deep layer input is biased away from non-FS interneurons (U = 59, p = 0.026, n = 14 pairs (FS), 5 pairs (non-FS), Mann Whitney).

q) Strategy to record local inhibitory input to superficial and deep vH neurons.

r) IPSCs in pairs of superficial and deep PFC-projecting (*top*) and neighboring non-PFC projecting (*bottom*) vH neurons. Scale bar = 20 ms and 0.5 deep response.

s) Summary of inhibitory connectivity. Inhibitory input is equivalent onto both superficial and deep PFC-projecting neurons (U = 57, p = 0.38, n = 17 pairs, Mann Whitney), but biased towards deep layer non-PFC projecting neurons (U = 10, p = 0.042, n = 11 pairs, Mann Whitney).

t) Strategy to investigate superficial and deep vH neuron connectivity onto local interneurons.

u) Focused light allows activation of neurons expressing soCoChR with high spatial resolution. Scale bar = 10 mV, 20 ms.

v) Connectivity of superficial and deep PFC projecting vH neurons onto neighboring *dlx+* interneurons. Amplitude of EPSCs and probability of connectivity is equivalent for both layers (Amplitude: U = 8, p = 0.42, n = 5 connected pairs, Mann Whitney; % connected: Odds ratio = 0.95, p = 1.0, n = 19 (Sup), n = 18 (Deep), Fishers Exact Test). Scale bar = 10 pA, 20 ms.

1

Interneurons in PFC can be characterized into two main subgroups – soma-targeting fast-spiking interneurons, and dendrite-targeting non-fast-spiking interneurons – based on their intrinsic properties and the expression of peptides such as parvalbumin and somatostatin[19] (***Sup.Fig.6***). We used CRACM to compare the relative input from superficial and deep layer vH neurons onto pairs of layer V PFC pyramidal neurons and neighboring interneurons identified by their electrophysiological and molecular properties (***Fig2m-p***). Deep layer vH neurons showed robust input onto both pyramidal neurons and neighboring fast-spiking interneurons in PFC, but very little input onto non-fast-spiking interneurons. In contrast, superficial vH input innervated both fast-spiking and non-fast-spiking interneurons in PFC. This suggests that the overall inhibitory bias of superficial vH input may be a result of widespread recruitment of both dendritic and somatic inhibitory circuits within PFC.

These results suggest a push-pull type circuit where superficial vH neurons inhibit PFC circuitry via broad recruitment of local interneurons, while deep layer neurons activate PFC via direct recruitment of pyramidal neurons. A hallmark of such circuit motifs in other brain regions is lateral inhibition across the two controlling populations. Consistent with this, we found that ChR2 mediated activation of PV+ interneurons in vH resulted in robust IPSCs in retrogradely labelled superficial and deep PFC-projecting neurons (***Fig2q-s***). This is in contrast to neighboring non-PFC-projecting neurons in which IPSCs were biased towards deep layer neurons[20]. To investigate the connectivity of each layer onto local interneurons, we elicited action potentials in individual PFC-projecting neurons from each layer while recording from neighboring genetically identified interneurons in vH, using a focused light spot to activate somatically targeted CoChR2 (***Fig.2t,u***). We found that PFC-projecting neurons in each layer connected to local interneurons with a similar amplitude and connection probability (***Fig.2v***). Overall, this suggests lateral inhibition across the two populations of vH-PFC neurons, completing a prototypical push-pull circuit.

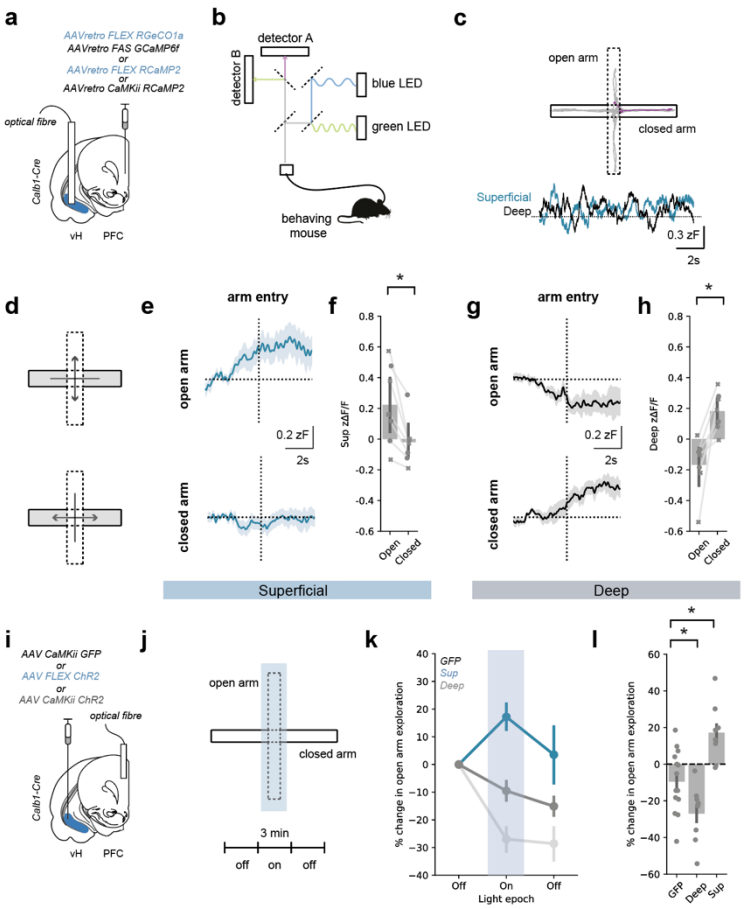

Figure 3 | Superficial and deep vH-PFC populations bidirectionally influence exploratory behavior.

a,b) Strategy to record superficial and deep vH-PFC neuron calcium dynamics during free behavior.

c) Example of simultaneously recorded calcium fluorescence from superficial (*blue*) and deep (*black*) neurons while the mouse navigated the EPM (corresponding position highlighted in *purple*).

d,e) Superficial calcium fluorescence aligned to open arm (*top*) and closed arm (*bottom*) entry. Superficial neurons responded only to open arm entry.

f) Summary of (**e**) showing superficial activity is greater on open arm entry compared to closed arm entry ($t_{(6)} = 3.65$, $p = 0.01$, $n = 7$ mice, Welch paired t-test with Holm-Sidak correction). Mice where superficial and deep activity were acquired simultaneously are plotted as (x) while mice where superficial and deep activity was acquired separately with the same sensor as a control are plotted as (o) (see methods, ***Sup.Fig.7***).

g,h) Deep layer neuron calcium fluorescence aligned to open (*top*) and closed (*bottom*) arm entry. Deep layer neurons respond to both open and closed arm entry. Fluorescence decreases upon open arm entry, and increases on closed arm entry, summarized in (**h**), markers as in (**f**) ($t_{(6)} = 4.13$, $p = 0.01$, $n = 7$ mice, Welch paired t-test with Holm-Sidak correction).

i) Strategy for *in vivo* optogenetic manipulation of vH axons from each layer in PFC.

j) Experimental design: after a 3 min baseline, for a second 3 min epoch 20 Hz light was delivered via the optical fiber when the mouse entered the center point of the maze, and continued until return to the closed arms. Mice then remained in the maze for a third post stimulation 3 min epoch.

k) Change in open arm exploration due to stimulation of superficial, deep or control axons in PFC. Stimulation dramatically altered exploration with superficial axon stimulation increasing and deep axon stimulation decreasing open arm exploration relative to controls (Interaction between group and epoch, $F_{(4,56)} = 4.36$, $p = 0.018$, $n = 15$ (GFP), $n = 8$ (Sup), $n = 8$ (Deep), 2-way repeated measures ANOVA).

l) Summary of stimulation-induced alteration to open arm exploration (GFP:Sup: $t_{(23)} = 3.78$, $p = 0.004$; GFP:Deep: $t_{(23)} = 2.48$, $p = 0.026$, n as above, Welch t-test with Holm-Sidak correction).

vH-PFC projecting neurons are strongly implicated in exploration of the elevated plus maze (EPM), where their activity tracks the decision to enter the potentially threatening open arms of the maze[2,5,7]. We next asked if the two opposing superficial and deep populations in vH were differentially active during this exploratory behavior, as suggested by their circuit connectivity. We recorded the activity of both populations using bulk calcium imaging through an optical fiber (***Fig.3a-c, Sup.Fig.7***). We aligned these recordings to when mice made the decision to move from the closed arms to the open arm of the elevated plus maze, and compared this to the decision to enter the closed arms of the maze (***Fig.3d***). We found that in the seconds leading up to exploration of the open arms of the maze, superficial neurons increased their activity. This activity was maintained for seconds after open arm entry. In contrast, upon entry to the closed arms of the maze, superficial neurons had no response (***Fig.3e,f***). Consistent with a dichotomy of function across the two vH populations, deep layer neurons showed opposing patterns of activity when compared to superficial neurons. Activity of deep layer neurons was reduced upon entry of the open arms, and increased upon entry of the closed arms (***Fig.3g,h***). Together this suggests that activity of the superficial layer may be associated with the decision to enter the open arm, while activity of the deep layer with the return to the closed arms.

To test if the observed activity of the two populations could influence exploratory choice, we expressed ChR2 in either deep or superficial layer neurons in vH, and implanted optical fibers unilaterally in PFC (***Fig.3i, Sup.Fig.8***). This allowed us to stimulate axons arriving in PFC from each of the two layers while the animal was exploring the maze. To mimic the activity from our calcium recordings, we artificially activated axons with blue light for a three-minute epoch, only when mice entered the central choice point in the EPM, and maintained excitation until the mice returned to the closed arms[1] (***Fig.3j***). Consistent with our calcium imaging data, activation of superficial layer vH axons in PFC promoted the exploration of the open arms compared to GFP expressing controls, while activating the deep layer vH axons in PFC reduced exploration of the open arms (***Fig.3k,l, Sup.Fig.8***).

Overall, we have identified two parallel populations of pyramidal neurons in the hippocampus that send projections to PFC. These two populations form a long-range push-pull circuit. One population is driven by top-down cortical input and promotes exploration via preferential recruitment of feedforward inhibition within PFC. The second is driven by bottom-up basal forebrain and thalamic input, and promotes avoidance via direct connections onto PFC pyramidal neurons (***Sup.Fig.9***). This push-pull circuit provides a mechanism for regulation of exploratory behavior through bidirectional hippocampal control of PFC, and provides a circuit basis for the control of the intricate excitatory and inhibitory circuit architecture of the PFC.

REFERENCES

1. Lee, A.T. et al. *Neuron* **102**, 1223–1234.e4 (2019).
2. Padilla-Coreano, N. et al. *Neuron* **89**, 857–866 (2016).
3. Padilla-Coreano, N. et al. *Neuron* **104**, 601–610.e4 (2019).
4. Parfitt, G.M. et al. *Neuropsychopharmacology* **42**, 1715–1728 (2017).
5. Ciocchi, S., Passecker, J., Malagon-Vina, H., Mikus, N. & Klausberger, T. *Science* **348**, 560–563 (2015).
6. Jadhav, S.P., Rothschild, G., Roumis, D.K. & Frank, L.M. *Neuron* **90**, 113–127 (2016).
7. Adhikari, A., Topiwala, M.A. & Gordon, J.A. *Neuron* **71**, 898–910 (2011).
8. Tang, W., Shin, J.D., Frank, L.M. & Jadhav, S.P. *J Neurosci* **37**, 11789–11805 (2017).
9. Spellman, T. et al. *Nature* **522**, 309–314 (2015).
10. Kjaerby, C., Athilingam, J., Robinson, S.E., Iafrati, J. & Sohal, V.S. *Cell Rep* **17**, 2882–2890 (2016).
11. Marek, R. et al. *Nat Neurosci* **21**, 384–392 (2018).
12. Shin, J.D. & Jadhav, S.P. *Curr Opin Neurobiol* **40**, 161–169 (2016).
13. Cembrowski, M.S. & Spruston, N. *Nat Rev Neurosci* **20**, 193–204 (2019).
14. Bienkowski, M.S. et al. *Nat Neurosci* **21**, 1628–1643 (2018).
15. Soltesz, I. & Losonczy, A. *Nat Neurosci* **21**, 484–493 (2018).
16. Li, Y. et al. *Nat Neurosci* **20**, 559–570 (2017).
17. Marek, R., Xu, L., Sullivan, R.K.P. & Sah, P. *Nat Neurosci* **21**, 654–658 (2018).
18. Mukherjee, A. & Caroni, P. *Nat Commun* **9**, 167 (2018).
19. The Petilla Interneuron Nomenclature Group (PING) *Nat Rev Neurosci* **9**, 557–568 (2008).
20. Lee, S.H. et al. *Neuron* **82**, 1129–1144 (2014).

STATISTICS SUMMARY

FIGURE	DESCRIPTORS	N	TEST USED	TEST STATISTIC	P VALUE
1g	ENT – superficial:deep ratio mean+/- sem	9 9	Wilcoxon paired	V = 44	p = 0.007
	CA3 - superficial:deep ratio mean+/- sem	10 10	Wilcoxon paired	V = 27	p = 1
	ATh - superficial:deep ratio mean+/- sem	7 7	Wilcoxon paired	V = 12	p = 0.034
	DBB – superficial:deep ratio mean+/- sem	15 15	Wilcoxon paired	V = 24	p = 0.041
2f	IL superficial: mean+/- sem deep: mean +/- sem	 4 4	 Mann Whitney	 U = 10	 p = 0.69
	PL superficial: mean+/- sem deep: mean +/- sem	 4 4	 Mann Whitney	 U = 4	 p = 0.34
	ORBm superficial: mean+/- sem deep: mean +/- sem	 4 4	 Mann Whitney	 U = 8	 p = 1
2i	CTXB superficial: mean+/- sem deep: mean +/- sem	 4 4	 Mann Whitney	 U = 4	 p = 0.3
	Rabies superficial: mean+/- sem deep: mean +/- sem	 4 4	 Mann Whitney	 U = 16.0	 p = 0.03
2l	Calb1: mean+/- sem CaMKii: mean +/- sem	10 8	Mann Whitney	U = 67	p = 0.018
2p	Calb1 Fast Spiking:pyramidal Non-fast spiking:pyramidal descriptor: mean+/- sem	 12 13	 Mann Whitney	 U = 84	 p = 0.77
	CaMKii Fast Spiking:pyramidal Non-fast spiking:pyramidal descriptor: mean+/- sem	 14 5	 Mann Whitney	 U = 59	 p = 0.026
2s	PFC+ superficial: mean+/- sem deep: mean +/- sem	 17 17	 Wilcoxon paired	 V = 57	 p = 0.38
	PFC- superficial: mean+/- sem deep: mean +/- sem	 11 11	 Wilcoxon paired	 V = 10	 p = 0.042

1

FIGURE	DESCRIPTORS	N	TEST USED	TEST STATISTIC	P VALUE
2v	Amplitude				
	superficial: mean+/- sem	5	Mann Whitney	U = 8	p = 0.42
	deep: mean +/- sem	5			
	% Connected				
	superficial: % of total	19	Fisher's exact test	Odds ratio = 0.95	p = 1.0
	deep: mean % of total	18			
3f	Sup				
	Open arms: mean+/- sem	7	Welch paired t-test with Holm-Sidak	$t_{(6)} = 3.65$	p = 0.01
	Closed arms: mean+/- sem	7	correction		
3h	Deep				
	Open arms: mean+/- sem	7	Welch paired t-test with Holm-Sidak	$t_{(6)} = 4.13$	p = 0.01
	Closed arms: mean+/- sem	7	correction		
3k	GFP	15	Two way repeated measures ANOVA		
	Superficial ChR2	8	Main effect of epoch	$F_{(2,56)} = 4.35$	p = 0.018
	Deep ChR2	8	Interaction of group x epoch	$F_{(4,56)} = 4.37$	p = 0.004
3l	GFP	15	Welch paired t-test with Holm-Sidak	$t_{(23)} = 3.78$	p = 0.004
	Superficial ChR2	8	correction		
	GFP	15	Welch paired t-test with Holm-Sidak	$t_{(23)} = 2.48$	p = 0.026
	Deep ChR2	8	correction		

METHODS

Animals

6 - 10 week old (adult) male and female C57 / bl6J mice provided by Charles River were used except where noted. To target inhibitory neurons we used the *Slc32a1(VGAT)-IRES-Cre* (#016962) knock-in line. To target Calbindin expressing neurons we used the *Calb1-IRES-Cre* (#028532) knock-in line. To target parvalbumin positive interneurons we used the *PV-IRES-Cre* (#008069) knock in line. All were obtained from Jackson laboratories and bred in-house. Mice were housed in cages of 2 - 4 and kept in a humidity- and temperature-controlled environment under a 12 h light/dark cycle (lights on 7 am to 7 pm) with ad-libitum access to food and water. All experiments were approved by the U.K. Home Office as defined by the Animals (Scientific Procedures) Act, and University College London ethical guidelines.

Stereotaxic surgery

Retrograde tracers:

Red and Green fluorescent retrobeads (Lumafluor, Inc.) for electrophysiological recordings.

Cholera toxin subunit B (CTXβ) tagged with Alexa 555 or 647 (Molecular Probes) for histology experiments.

Viruses:

AAV2/1-CaMKII-GFP	(a gift from Edward Boyden; Addgene plasmid #64545)
AAV1.CAG.FLEX.Ruby2sm-Flag.WPRE	(a gift from Loren Looger; Addgene plasmid #98925, see ref[21])
AAVretro-Ef1a-DO_DIO-TdTomato_EGFP	(a gift from Bernardo Sabatini; Addgene plasmid #37120, see ref[22])
AAV2retro-CAG-Cre	(UNC vector core)
AAV2/1-CaMKii-Cre	(UNC vector core)
AAV2/1-synP-FLEX-split-TVA-EGFP-B19G	(a gift from Ian Wickersham; Addgene plasmid #52473, see ref[23])
EnvA-ΔG-RABV-H2B-mCherry-2A-CLIP	(a gift from Marco Tripodi, LMB, Cambridge, UK)
AAV2/1-EF1a-FLEX-hChR2(H134R)-EYFP	(a gift from Karl Deisseroth; Addgene viral prep #20298-AAV1)
AAV2/1-hSyn-hChR2(H134R)-EYFP	(a gift from Karl Deisseroth; Addgene viral prep #26973-AAV1)
AAV2/1-CaMKIIa-hChR2(H134R)-EYFP	(a gift from Karl Deisseroth; Addgene viral prep #26969-AAV1, see ref[24])
AAV2/9-mDlx-NLS-mRuby2	(a gift from Viviana Gradinaru; Addgene viral prep #99130-AAV1, see ref[25])
pAAV2/9-hSynapsin-FLEX-soCoChR-GFP	(a gift from Edward Boyden, Addgene viral prep #107712-AAV9, see ref[26])
AAVretro.Syn.Flex.NES-jRGECO1a.WPRE	(a gift from Douglas Kim & GENIE Project; Addgene viral prep #100853-AAVrg, see ref[27])
AAVretro.CAG.FAS.GCaMP6f.WPRE	(Vectorbuilder)
AAVretro.CAG.FLEX.RCaMP2.WPRE	(UNC vector core)
AAVretro.CaMKii.RCaMP2.WPRE	(UNC vector core)

Surgery:

Stereotaxic injections were performed on 7 - 10 week old mice anaesthetized with isofluorane (4 % induction, 1 - 2 % maintenance) and injections carried out as previously described[28-30]. Briefly, the skull was exposed with a single incision, and small holes drilled in the skull directly above the injection site. Injections are carried out using long-shaft borosilicate glass pipettes with a tip diameter of ~ 10 - 50 µm. Pipettes were back-filled with mineral oil and front-filled with ~ 0.8 µl of the substance to be injected. A total volume of 140 - 160 nl of each virus was injected at each location in ~ 14 or 28 nl increments every 30 s. If two or more substances were injected in the same region they were mixed prior to injection. The pipette was left in place for an additional 10 min to minimize diffusion and then slowly removed. If optic fibers were also implanted, these were inserted immediately after virus injection, secured with 1 – 2 skull screws and cemented in place with C&B superbond. Injection coordinates were as follows (mm relative to bregma):

infralimbic PFC:	ML: ± 0.4,	RC: + 2.3,	and DV: - 2.4,
Diagonal band of Broca:	ML: ± 0.2,	RC: + 0.7,	and DV: - 4.0,
anterior thalamus:	ML: ± 0.2,	RC: - 0.4,	and DV: - 3.2,
CA3:	ML: ± 2.8,	RC: - 3.0,	and DV: - 4,
Entorhinal cortex:	ML: ± 2.7,	RC: - 5.2 (@ 10 °),	and DV: - 4.5,
ventral hippocampus:	ML: ± 3.4,	RC: - 3.7,	and DV: - 4.3.

After injection, the wound was sutured and sealed, and mice recovered for ~30 min on a heat pad before they were returned to their home cage. Animals received carprofen in their drinking water (0.05 mg / ml) for 48 hrs post-surgery as well as subcutaneously following surgery (0.5 mg / kg). Expression occurred in the injected brain region for ~2 weeks until preparation of acute slices for physiology experiments, or fixation for histology. The locations of injection sites were verified for each experiment.

Anatomy

Pseudotyped rabies labelling from PFC:
For pseudotyped rabies experiments two injections were necessary. First, *AAV2/1-synP-FLEX-split-TVA-EGFP-B19G* was injected into the PFC of either *VGAT-Cre* mice to express TVA and G protein in inhibitory neurons, or was coinjected in a 1:1 mixture with *AAV2/1-CaMKii-Cre* into Cre negative littermates to label excitatory neurons. In addition, CTXβ was coinjected into PFC to achieve non-specific retrograde labelling for comparison across mice. 2 weeks later, 200 nl of *EnvA-ΔG-RABV-H2B-mCherry* was injected into PFC to infect and induce transynaptic spread only in neurons expressing Cre. Animals were prepared for histology after 7 days of rabies-mediated expression.

TRIO labelling from PFC-projecting vH neurons:
TRIO labelling[31] again required two surgeries. First, *AAVretro-CAG-Cre* (UNC) was injected into the PFC to express Cre recombinase in neurons projecting to PFC. In the same surgery *AAV2/1-synP-FLEX-split-TVA-EGFP-B19G* (UNC) was injected into the vH to express rabies TVA and G-protein only in vH neurons that express Cre (i.e. only those that project to PFC). 2 weeks later, 200 nl of *EnvA-ΔG-RABV-H2B-mCherry* was injected into vH to infect and induce trans-synaptic spread only in PFC-projecting vH neurons. Animals were prepared for histology after 7 days of rabies-mediated expression.

Histology:
Mice were perfused with 4% PFA (wt / vol) in PBS, pH 7.4, and the brains dissected and postfixed overnight at 4ºC as previously described[28,30]. 70 µm thick slices were cut using a vibratome (Campden Instruments) in either the transverse, coronal or sagittal planes as described in the figure legends. Slices were mounted on Superfrost glass slides with ProLong Gold or ProLong Glass (for visualization of GFP) antifade mounting medium (Molecular Probes). NucBlue was included to label gross anatomy. Imaging was carried out with a Zeiss Axio Scan Z1, using standard filter sets for excitation/emission at 365-445/50 nm, 470/40-525/50 nm, 545/25-605/70 nm and 640/30-690/50 nm. Raw images were analyzed with FIJI.

Immunohistochemistry:
Brain slices for staining were prepared as described above. Firstly, 70 µm thick slices were incubated in blocking solution (0.03 % BSA and 0.5 % triton in PBS) for 3 hours at room temperature. Following incubation in blocking solution, slices were incubated overnight in a 1:5000 dilution of anti-DDDDK Tag primary antibody (ab1257, Abcam) in blocking solution at 4 °C. Following incubation in primary antibody, slices were washed 3 times (30 minutes per wash) in PBS before incubation in a 1:500 dilution of secondary antibody (Alexa 555 donkey anti-goat; A21432, Invitrogen) for 4 hours at room temperature. Following this incubation, slices were washed again in PBS as before and mounted (as above) for imaging.

Analysis of spatial distribution of PFC-projecting hippocampal neurons:
The spatial distribution of retrogradely labelled PFC-projecting hippocampal neurons was analyzed in transverse slices from mice injected with cholera toxin in PFC, and imaged as described above. 3 slices spanning 300µm between ~-3.5 and -5.0 mm DV were analyzed per injection. Sections containing the hippocampus were straightened along the cell body layer using the straighten macro in FIJI to produce a single field stretching from proximal CA3 to distal subiculum. Labelled cells within each slice were manually counted, and the coordinates saved for later analysis. We defined the CA1 / subiculum border as the point where the hippocampal cell layer widens into a more subicular-like structure, which occurs consistently at ~0.7 of the distance of the entire straightened field. Custom scripts written in Python based around the scikit.learn package were used to cluster the coordinates using a Gaussian Mixture Model (GMM). Models containing between 1 and 6 components were fit to the data, and Bayesian Information Criterion (BIC) was used to select the best fit.

Analysis of rabies labelling from VGAT and CaMKii neurons in PFC:
As above, transverse hippocampal slices containing cholera toxin and rabies labelling of PFC-projecting cells were used for cell counting. All cells in the straightened hippocampal formation were counted, irrespective of fluorescent label to gain an overall distribution of vH-PFC neurons. These coordinates were clustered using GMM as above, where all analyzed fields were best fit by two components. Rabies positive cells were assigned to one of the two components (i.e. superficial and deep layers) created by the clustering algorithm. Data is presented as proportion of all rabies labelled cells in each layer. As an internal control data for cholera toxin labelling is also presented using the same method, which shows there are no differences in the overall layer structure between the *CaMKii* and *VGAT* experiments.

Electrophysiology

Slice preparation:
Hippocampal recordings were studied in acute transverse slices, while prefrontal cortical recordings in ***Fig.2*** were studied in acute coronal slices. Mice were anaesthetized with a lethal dose of ketamine and xylazine, and perfused intracardially with ice-cold external solution containing (in mM): 210 sucrose, 7 glucose, 25 $NaHCO_3$, 1.25 NaH_2PO_4, 2.5 KCl, 1 Na^+ ascorbate, 3 Na^+ pyruvate, 7 $MgCl_2$ and 0.5 $CaCl_2$, bubbled with 95% O_2 and 5% CO_2. Slices (300 µm thick) were cut in this solution and then transferred to artificial cerebrospinal fluid (aCSF) containing (in mM): 119 NaCl, 25 glucose, 25 $NaHCO_3$, 1.25 NaH_2PO_4, 3 KCl,

1 Na+ ascorbate, 4 Na+ pyruvate, 1 $MgCl_2$ and 1.3 $CaCl_2$, bubbled with 95% O_2 and 5% CO_2. After 30 min at 35 °C, slices were stored for 30 min at 24 °C. All experiments were conducted at room temperature (22–24 °C). All chemicals were from Sigma, Hello Bio or Tocris.

Whole-cell electrophysiology:

Whole-cell recordings were made from hippocampal pyramidal neurons retrogradely labelled with retrobeads or CTXβ, which were identified by their fluorescent cell bodies and targeted with Dodt contrast microscopy, as previously described[28-30]. For sequential paired recordings, neurons were identified within a single field of view at the same depth into the slice. The recording order was counterbalanced to avoid any potential complications that could be associated with rundown. For current clamp recordings, borosilicate recording pipettes (2– 3 MΩ) were filled with (in mM): 135 K-gluconate, 10 HEPES, 7 KCl, 10 Na-phosphocreatine, 10 EGTA, 4 MgATP, 0.3 NaGTP). For voltage clamp experiments, three internals were used, First, in ***Fig.2j-l*** and ***Fig.2v***, Cs-gluconate based internal was used containing (in mM): 135 Gluconic acid, 10 HEPES, 7 KCl, 10 Na-phosphocreatine, 4 MgATP, 0.3 NaGTP, 10 TEA and 2 QX-314. In ***Fig.2j-l***, excitatory and inhibitory currents were electrically isolated by setting the holding potential at -70 mV (excitation) and 0 mV (inhibition) and recording in the presence of 10 mM extracellular APV, in ***Fig.2v*** excitatory currents were isolated by recording at – 70 mV in 10 mM extracellular Gabazine. Second, to allow characterization of interneuron intrinsic properties, experiments in ***Fig.2m-p*** were carried out using current clamp internal and excitatory currents were isolated using 10 mM extracellular Gabazine. Finally, to record inhibitory currents at rest in ***Fig.2q-s***, we used a high chloride internal (in mM): 135 CsCl, 10 HEPES, 7 KCl, 10 Na-phosphocreatine, 10 EGTA, 4 MgATP, 0.3 NaGTP, 10 TEA and 2 QX-314, with 10 mM external NBQX and 10 mM external APV. For two-photon experiments, the internal solution also contained 30 µM Alexa Fluor 594 (Molecular probes). Recordings were made using a Multiclamp 700B amplifier, with electrical signals filtered at 4 kHz and sampled at 10 kHz.

Viral strategy for in vitro optogenetics:

Presynaptic glutamate release was triggered by illuminating ChR2 in the presynaptic terminals of long-range inputs into the slice, as previously described[28-30]. Wide-field illumination was achieved via a 40 x objective with brief (0.2, 0.5, 1, 2 and 5 ms) pulses of blue light from an LED centered at 473 nm (CoolLED pE-4000, with appropriate excitation-emission filters). Light intensity was measured as 4–7 mW at the back aperture of the objective and was constant between all cell pairs.

To achieve afferent specific terminal stimulation in vH (***Fig.1e***), AAV2/1-hSyn-hChR2(H134R)-EYFP was injected into each downstream area, and retrobeads were injected into PFC to label the two layers in vH.

To achieve input-specific terminal stimulation in PFC (***Fig.2j-p*** and ***Fig3j-l***), we injected AAV2/1-EF1a-FLEX-hChR2(H134R)-EYFP in *Calb1-Cre* mice to target superficial neurons, and AAV2/1-CaMKIIa-hChR2(H134R)-EYFP to target deep layer neurons (see ***Sup.Fig.6*** for quantification of layer distribution).

To target whole cell recordings to interneurons (***Fig.2m,t, Fig.2v***), we used AAV2/9-dlx-mRuby injections in the area of interest.

To express ChR2 in local PV interneurons within vH (***Fig.2q***), we injected AAV2/1-EF1a-FLEX-hChR2(H134R)-EYFP into the vH of PV-Cre mice, and retrobeads into PFC to allow paired recordings from the two layers.

To allow single cell optogenetic stimulation (***Fig.2t-v***), we used an injection of AAVretro-syn-Cre in PFC, and an injection of AAV-EF1a-DIO-SoCoChR in vH. The resultant spare labelling of neurons across each layer allowed stimulation of individual SoCoChR expressing neurons with a focused light spot (with an activation resolution of ~50 µm ***Fig.2u***), while recording from neighboring interneurons labelled with dlx-mRuby as above.

2 photon imaging and image reconstruction:

Two-photon imaging was performed with a customized Slicescope (Scientifica), based on a design previously described[28-30]. For two-photon imaging, 780 nm light from an Erbium fiber laser (Menlo Systems) was used to excite Alexa Fluor 594. For each experiment a high-resolution stack of the entire neuron was taken for reconstruction of dendrite morphology.

Electrophysiology data acquisition and analysis:

Two-photon imaging and physiology data were acquired using National Instruments boards and SciScan (Scientifica) and WinWCP (University of Strathclyde) respectively. Electrical stimulation was via a tungsten bipolar electrode (WPI) and an isolated constant current stimulator (Digitimer). Optical stimulation was via wide field irradiance with 473 nm LED light (CoolLED) as described above. Data was analyzed using custom routines written in Python 3.6. Current step data was analyzed using routines based around the Neo and eFEL packages. For synaptic connectivity experiments, amplitudes of PSCs and PSPs were taken as averages over a 2-ms time window around the peak. For connectivity analysis, a cell was considered connected if the light-induced response was greater than 6 times the standard deviation of baseline.

Two-photon image reconstruction and analysis was carried out using VIAS and NeuronStudio[32], before further analysis was carried out using custom scripts in Python 3.6 based on the NeuroML package from the Human Brain Project. The online Human Brain Project morphology viewer was used for visualizing reconstructed neurons.

RNA Sequencing

Four 6 - 8 week old mice were injected with red retrobeads in PFC (see *surgery*). After 2 weeks, acute, 400 µm thick transverse hippocampal slices were prepared and incubated for 30 minutes at 35 ºC in oxygenated aCSF as above (see *electrophysiology*)

containing TTX (100 nM) to block sodium channels, NBQX (20 μM) and APV (50 μM) to block AMPA and NMDA receptor transmission respectively, and Pronase (1 mg / ml) to disrupt the extracellular matrix, followed by a further 30 mins wash in aCSF without Pronase. Following incubation, slices were placed in a sylgard-filled chamber under a dissection stereomicroscope (Leica MZ16FA) equipped with fluorescence and transmitted light. The ventral CA1 / subiculum was separated from the rest of the slice, and a single cut was made to separate superficial and deep cell layers, guided by the fluorescence of PFC-projecting cells. Superficial and deep excised sections from each animal were then pooled (4 samples of superficial and deep sections per animal), and tissue was manually triturated for dissociation using three glass Pasteur pipettes of decreasing tip diameter. The resulting suspension was mixed with DAPI (Molecular Probes) to monitor cell health, and then separated using FACS (UCL FACS facility) to isolate red fluorescent (PFC-projecting), and viable (DAPI negative) cells in superficial and deep layers. Cells were sorted directly into buffer for SMART-Seq v4 Ultra Low Input RNA Kit (Clontech Laboratories, Inc.). Subsequent processing was carried out by the UCL Genomics sequencing facility. Briefly, SMART (Switching Mechanism at 5' End of RNA Template) technology produces full-length PCR amplified cDNA starting from low input (as low as a single cell). 12 cycles of PCR were used to generate cDNA from lysed cells. The amplified cDNA was checked for integrity and quantity on the Agilent Bioanalyser using the High Sensitivity DNA kit. 200pg of cDNA was then converted to sequencing library using the Nextera XT DNA protocol (Illumina, San Diego, US). This uses a transposon able to fragment and tag double-stranded cDNA (tagmentation), followed by a limited PCR reaction (12 cycles) adding sample specific indexes to allow for multiplex sequencing. For sequencing, libraries to be multiplexed in the same run are pooled in equimolar quantities, calculated from Qubit and Tapestation fragment analysis. Samples were sequenced on the NextSeq 500 instrument (Illumina, San Diego, US) using a 43bp paired end run, generating approximately 200M read pairs in total. Fragments Per Kilobase Million (FPKM) scores were calculated from the raw data using TopHat and Cufflinks via Illumina Basespace software. Only raw FKPM scores over 10 were included. Due to the manual nature of the dissection, for identification of robust markers for the two layers, only hits where the standard deviation across samples in the two conditions was under 1 were included in final analysis. Statistical significance was compared across superficial and deep samples using false discovery rate correction and hits were defined as those where $q < 0.1$. The distribution along the radial axis of the hippocampus of a selection of hits were verified using in situ hybridization data from the Allen Brain Atlas[33].

Behavior

After sufficient time for surgical recovery and viral expression (>4 weeks), mice underwent multiple rounds of habituation. Mice were habituated to the behavioral testing area in their home cage for 30 min prior to testing each day. Mice were habituated to handling for at least 3 days, followed by 1-2 days of habituation to the optical tether in their home cage for 10 min.

Bulk calcium imaging using fiber photometry during elevated plus maze exploration:

Labelling superficial and deep vH neurons for photometry. Two strategies were employed to target superficial and deep vH-PFC neurons for photometry recordings. First, to allow simultaneous recordings of both populations, AAVretro-DIO-RGeCO1a and AAVretro-FAS-GCaMP6f were coinjected into PFC of *Calb1-Cre* mice as a 50:50 mix, and a 2.5 mm ferrule containing a 200 μm optical fiber was implanted in vH. This strategy allowed dual color imaging, as the red sensor RGeCO1a is expressed in superficial neurons, while the green sensor GCaMP6f is expressed in deep neurons in vH. FAS was used to counteract known interference between different Cre-dependent viruses[34]. Second, we repeated recordings in *Calb1-Cre* mice that were injected with either AAVretro-DIO-RCaMP2 to label superficial neurons, or AAVretro-CaMKii-RCaMP2 to label deep neurons. This strategy allowed us to use the same sensor (RCaMP2) to record activity of each population, to control for the possibility of potential interactions between, or any variability across sensors. As data did not differ across the two recording conditions (***Sup.Fig.7***), signals were pooled for further analysis.

Bulk calcium imaging during behavior. After habituation (above), mice were exposed to the elevated plus maze (EPM) for 9 min, and allowed to freely explore the open and closed arms of the maze. To record calcium activity, we used a system based on [35-37]. Briefly, two excitation LEDs (565 nm 'green' and 470nm 'blue') were controlled via a custom script written in Labview (National Instruments). Blue excitation was sinusoidally modulated at 210Hz and passed through a 470 nm excitation filter while green excitation was modulated at 500 Hz and passed through a 565 nm bandpass filter. Excitation light from each LED was collimated, then combined using a 520 nm long-pass dichroic mirror. The excitation light was coupled into a high-NA (0.53), low-autofluorescence 200 μm patch cord by reflection with a multiband dichroic mirror and fiber coupler. Each LED was set to 100 μW at the far end of the patch cord, which was terminated with a 2.5 mm ferrule. The emission signal was collected through the same patch cord and collimator, and separated from the excitation light by the multiband dichroic. Green and red signals were split using a longpass dichroic mirror before being passed through a GFP emission filter and RFP emission filter respectively. Filtered emission was then collected by a femtowatt photoreceiver (Newport). The photoreceiver signal was sampled at 100 kHz, and each of the two modulated signals generated by the two LEDs was independently recovered using standard synchronous demodulation techniques implemented in real time by a custom Labview script. Three separated signals; green, red and autofluorescence (the signal from each sensor at the modulation frequency that does not match the sensor), were then downsampled to 50 Hz before being exported for further analysis. A least-squares linear fit was applied to the autofluorescence signal to align it to the green and red signals. Time series data was then calculated for each behavioral session as the zscore of (green or red signal - fitted autofluorescence signal). Calcium signals around open versus closed arm entries were then calculated by aligning normalized traces to timestamps from automated video analysis (Ethovision, Noldus). Activity was analyzed as the area under the curve from 0 to 4 s after arm entry, normalized to the area under the curve -4 to -2 s before arm entry. All optical components were from Thorlabs, Semrock or Chroma, patch cords were from Doric Lenses.

Optogenetic manipulation of neurons during elevated plus maze exploration:
Axon terminals in PFC from superficial and deep vH neurons were labelled as described above (see ***Optogenetics***), and a 200 µm optical fiber was implanted unilaterally above right PFC. Mice expressing GFP in vH were used as controls. After habituation (above), behavior was assessed using the EPM. As above, EPM sessions lasted 9 min. For stimulation, the session was split into 3, 3 min epochs. 20 Hz light stimulation was delivered via a 473 nm laser, coupled to a patch cord (6-8 mW at the end of the patch cord) during the second three-minute epoch to activate ChR2 positive vH terminals in PFC. To mimic activity observed in calcium recordings, real-time light delivery was based on the location of the mouse in the EPM apparatus, where light stimulation occurred only during points where the mouse was in the center or open arms of the maze[1,38]. Time spent investigating the open arms of the maze was scored for each mouse in each epoch by an experimenter blinded to the injected virus.

Statistics
Summary data are reported throughout the text and figures as the mean ± s.e.m, unless stated otherwise. Physiology and imaging data were assessed using statistical tests described in the figure legends, and in the supplementary statistics summary. Significance was defined as $P < 0.05$, all tests were two sided. No statistical test was run to determine sample size a priori. The sample sizes we chose are similar to those used in previous publications. Animals were randomly assigned to a virus cohort (e.g. ChR2 versus GFP), and where possible the experimenter was blinded to each mouse's virus assignment when the experiment was performed. This was sometimes not possible due to e.g. the presence of the injection site in the recorded slice.

ACKNOWLEDGEMENTS

We thank Marco Tripodi for providing rabies virus, and the UCL FACS facility and UCL Genomics for help with RNA sequencing. We thank David Attwell, Francesca Cacucci, Mark Farrant, Tara Keck, Troy Margrie, Aman Saleem, Andreas Schaefer, Marcus Stephenson-Jones, and members of the MacAskill laboratory for helpful comments on the manuscript. A.F.M. was supported by a Sir Henry Dale Fellowship jointly funded by the Wellcome Trust and the Royal Society (grant number 109360/Z/15/Z) and by a UCL Excellence Fellowship. C.S.B. was supported by the Wellcome Trust 4-year PhD in Neuroscience at UCL (grant number 206074/Z/17/Z).

AUTHOR CONTRIBUTIONS

C.S.B and A.F.M collected the data, C.S.B analyzed the data with input from A.F.M. C.S.B and A.F.M wrote the manuscript.

SUPPLEMENTARY ONLINE REFERENCES

21. Viswanathan, S. et al. *Nat Methods* **12**, 568–576 (2015).
22. Saunders, A., Johnson, C.A. & Sabatini, B.L. *Front Neural Circuits* **6**, 47 (2012).
23. Kohara, K. et al. *Nat Neurosci* **17**, 269–279 (2014).
24. Lee, J.H. et al. *Nature* **465**, 788–792 (2010).
25. Chan, K.Y. et al. *Nat Neurosci* **20**, 1172–1179 (2017).
26. Shemesh, O.A. et al. *Nat Neurosci* **20**, 1796–1806 (2017).
27. Dana, H. et al. *Elife* **5**, 413 (2016).
28. Macaskill, A.F., Cassel, J.M. & Carter, A.G. *Nat Neurosci* **17**, 1198–1207 (2014).
29. Little, J.P. & Carter, A.G. *J Neurosci* **33**, 15333–15342 (2013).
30. Macaskill, A.F., Little, J.P., Cassel, J.M. & Carter, A.G. *Nat Neurosci* **15**, 1624–1626 (2012).
31. Schwarz, L.A. et al. *Nature* **524**, 88–92 (2015).
32. Dumitriu, D., Rodriguez, A. & Morrison, J.H. *Nat Protoc* **6**, 1391–1411 (2011).
33. Lein, E.S. et al. *Nature* **445**, 168–176 (2007).
34. Beier, K.T., Saunders, A.B., Oldenburg, I.A., Sabatini, B.L. & Cepko, C.L. *Front Neural Circuits* **7**, 11 (2013).
35. Lerner, T.N. et al. *Cell* **162**, 635–647 (2015).
36. Kim, C.K. et al. *Nat Methods* **13**, 325–328 (2016).
37. Markowitz, J.E. et al. *Cell* **174**, 44–58.e17 (2018).
38. Jimenez, J.C. et al. *Neuron* **97**, 670–683.e6 (2018).

SUPPLEMENTARY FIGURES

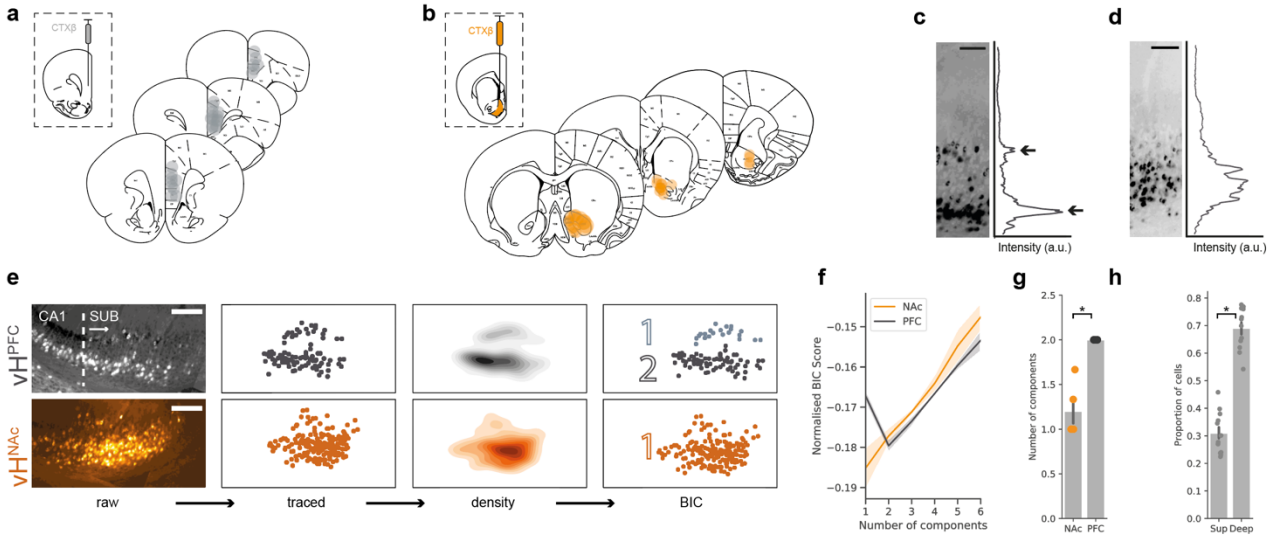

Supplementary Figure 1. Retrograde labelling and clustering of projection populations.

a) Schematic of CTXβ injection into PFC and location of injections (n = 16). Each injection is represented as a transparent fill. Thus, higher intensity reflects consistent labelling across injections.

b) as in (**a**) but for injections into the NAc (n = 12).

c,d) Example fields of retrogradely labelled neurons in transverse slices of vH after CTXβ injection into PFC (**c**) and NAc (**d**). Profile on right indicates fluorescence intensity profile along the radial axis. Note PFC-projecting neurons have two peaks, while NAc has one. Scale Bars = 100µm.

e) Locations of neuron coordinates were clustered using a Gaussian Mixture Model (GMM). Models containing between 1 and 6 components were fit to the data, and Bayesian Information Criterion (BIC) was used to select the best fit. Figure shows example of clustering of spatial location of both PFC-projecting neurons (which consistently form two layers) and NAc projecting neurons (which consistently form a single cluster in the centre of the cell body layer, between the two PFC layers). Images from left to right show raw images, coordinates of neuronal cell bodies, a heat map showing the density of cell bodies and the neuronal cell bodies colour coded according to the groups that gave the best BIC score (2 components for PFC in grey and black, one component for NAc in orange). See (**f**) for quantification. Scale Bars = 100µm.

f) BIC scores for positions of PFC (grey) and NAc (orange) projecting neurons for 1 – 6 components.

g) Summary of component number that gave the lowest BIC score across all experiments. Note PFC projectors are consistently fit best by two components, while NAc projectors are best fit by 1 component.

h) Summary of proportion of PFC-projecting neurons in each component (superficial and deep layers), quantified from CTXβ-labelled neurons. Note that roughly 70% of the projection population is composed of deep-layer neurons. Grey dots represent brain slices quantified from 4 injections.

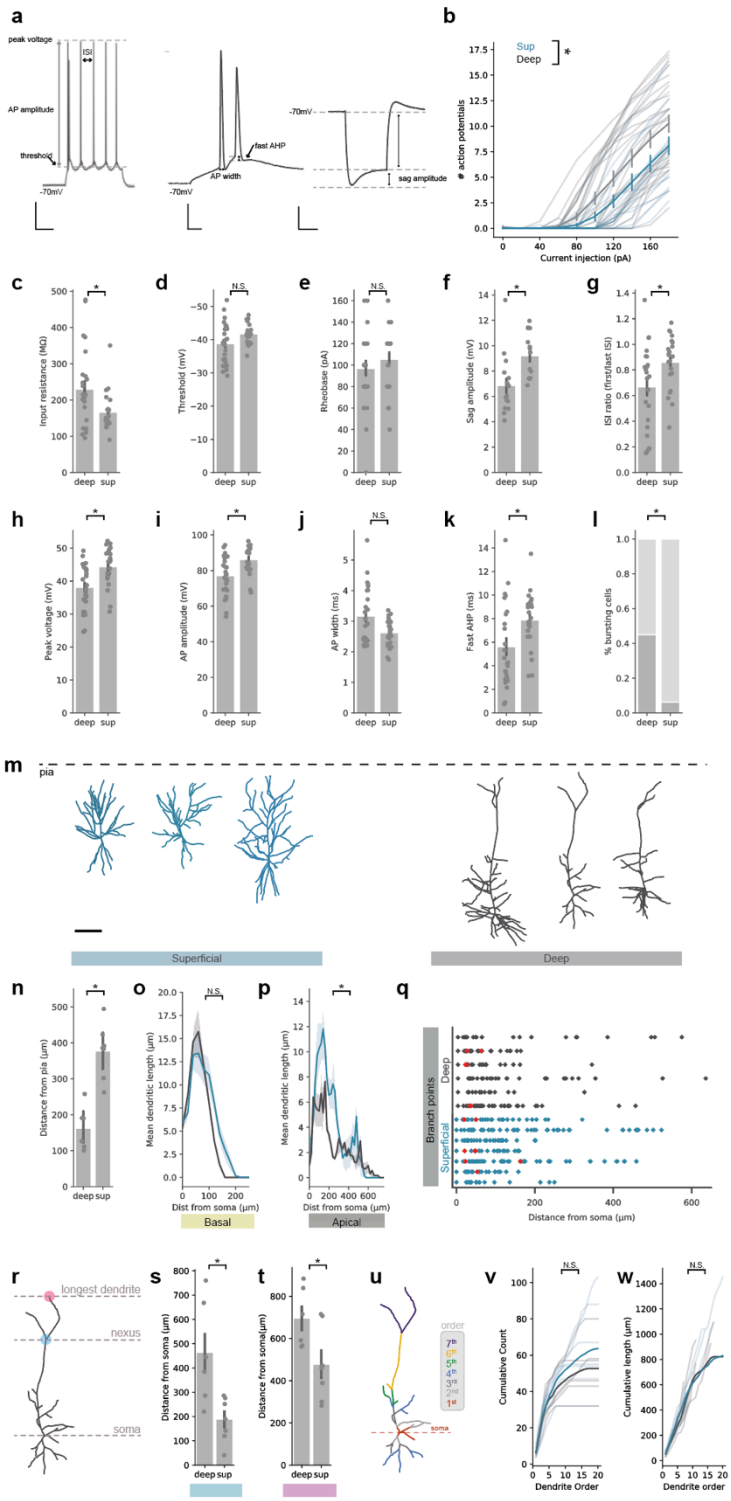

Supplementary Figure 2. Characterization of superficial- and deep-layer electrophysiological and morphological properties

a) Example voltage traces from a deep layer PFC-projecting cell in response to current injections (140 pA for the first two traces and -160 pA for the last trace). The middle trace is a zoom in of the first two events of the first trace. Arrows point at different aspects of the traces analyzed below. Sacle bars = 100 ms, 20 mV; 10 ms, 20 mV; 200 ms, 10 mV. [scale preemptively corrected based on ai file]

b-l) Electrophysiological properties of n = 22 cells (superficial), 26 cells (deep) from 12 and 16 animals respectively for all measures.

m) Example reconstructions of superficial (blue) and deep (dark grey) PFC-projecting hippocampal neurons. Scale bar = 100 µm, dotted line represents pia.

n) Quantification of distance of recorded neurons in deep and superficial layers from the basal pia (towards dentate gyrus).

o) Sholl analysis of basal dendritic length with increasing distance from the soma for superficial (blue) and deep (black) neurons.

p) as in (**o**) but for apical dendritic length.

q) Distribution of branch points with increasing distance from the soma in superficial (blue) and deep (black) layer neurons. Red points indicate two branch points in the same bin.

r) Schematic illustrating further characterization of the apical dendrite: the nexus (the base of the tuft where the apical dendrite splits) and the position of the dendrite tip farthest away from the soma.

s) Quantification of the distance from the nexus to the soma in superficial and deep neurons.

t) Quantification of the distance from the farthest dendrite tip to the soma.

u) Schematic illustrating branching order in a sample deep layer pyramidal neuron.

v) Quantification of cumulative number and cumulative length (**w**) of dendrites at each centrifugal dendritic order.

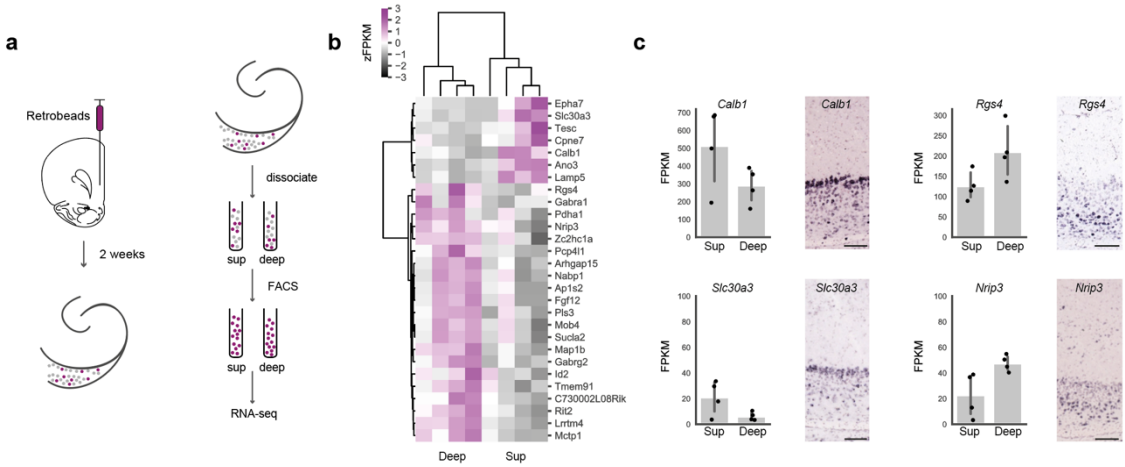

Supplementary Figure 3. RNA sequencing of deep and superficial layer PFC-projecting vH neurons.

a) Schematic of strategy to isolate retrogradely labelled neurons from each layer. Transverse slices were manually dissected down the middle of the cell body field and labelled cells were isolated using FACS before undergoing RNA sequencing.

b) Hierarchical clustering of genes with differential expression across the two groups, showing enrichment of genes in both superficial and deep populations across 4 biological replicates (n = 4 dissected hippocampi). Colour is scaled based on a row-wise Z score of the FPKM value.

c) Validation of example genes. For each example, raw FPKM scores are plotted for superficial and deep layers on the left, and in-situ hybridisation (ISH) data of vH from Allen brain atlas on the right. Note for each hit, ISH data recapitulate either superficial or deep enrichment of gene expression. Scale bars = 100 μm.

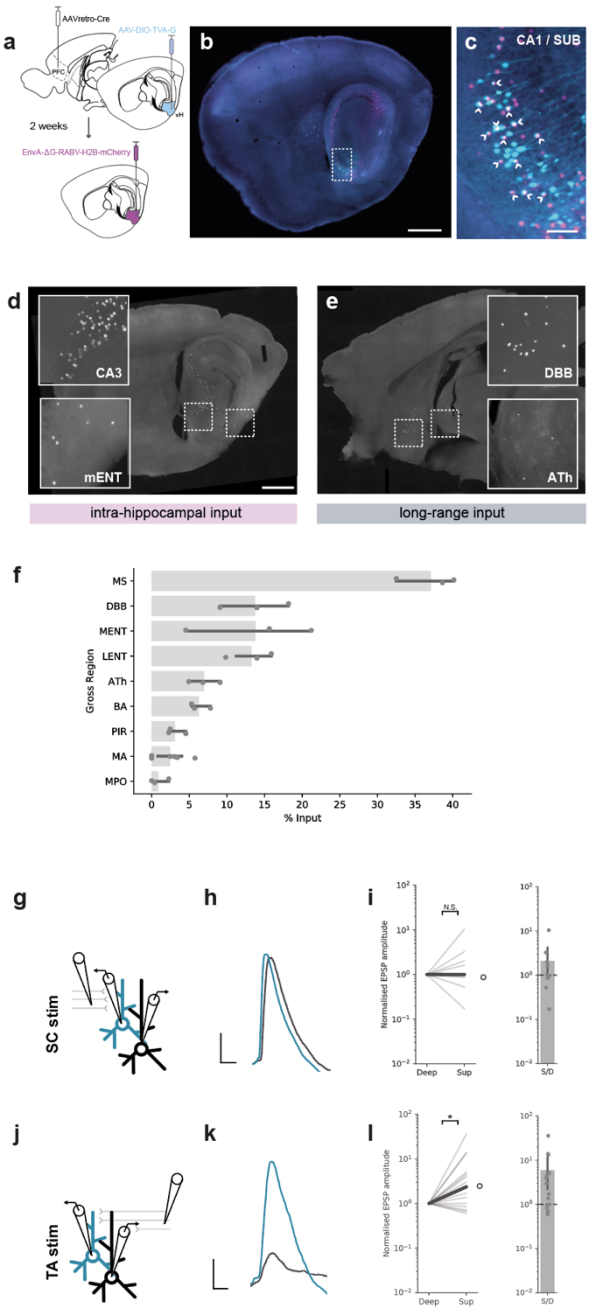

Supplementary Figure 4. Quantification of TRIO-labelled inputs and electrically stimulated validation of CA3 and ENT inputs

a) Schematic of TRIO injection strategy. *AAVretro-CAG-Cre* was injected in PFC, and rabies helper proteins were injected into vH to limit subsequent rabies infection to hippocampal PFC projection neurons. 2 weeks later, EnvA pseudotyped rabies was injected in vH to label presynaptic neurons that synapse onto PFC-projecting hippocampal neurons with nuclear-localized mCherry.

b) Injection site in a sagittal section showing TVA and G protein expressing hippocampal neurons (cyan), and rabies labelled neurons (magenta). Scale bar = 1000 µm.

c) Zoom in to white dotted box in (**b**). Co-labelled neurons represent starter neurons (arrows). Scale bar = 100 µm.

d) Sagittal section showing insets of rabies-labelled cells in intra-hippocampal input regions CA3 and mENT. Scale bar = 1000µm.

e) Sagittal section showing insets of rabies-labelled cells in extra-hippocampal input regions DBB and ATh. Scale bar = 1000µm.

f) Quantification of % input into vH from a variety of regions. Note that MS, DBB, mENT and ATh (hits followed up in ***Fig.1***) are on the upper end of the scale, contributing high amounts of input to vH.

g) Schematic of experimental setup showing electrical stimulation of Schafer Collaterals (SC) axons while recording from either superficial (blue) or deep (black) PFC-projecting cells.

h) Representative EPSP traces in response to 0.5 mA SC stimulation

i) *Left*, Normalized EPSP amplitude (to the amplitude of response in the deep cell) per pair of recorded cells. Note that, as with light evoked stimulation of contralateral CA3 terminals, SC inputs are not biased towards either population of cells. *Right*, Summary of EPSP amplitude ratios. Dotted line represents a ratio of 1.

j-l) As above but for Temporoamonic (TA) axon stimulation. Note that, as with light evoked stimulation of ENT terminals, TA inputs are biased towards superficial layer cells.

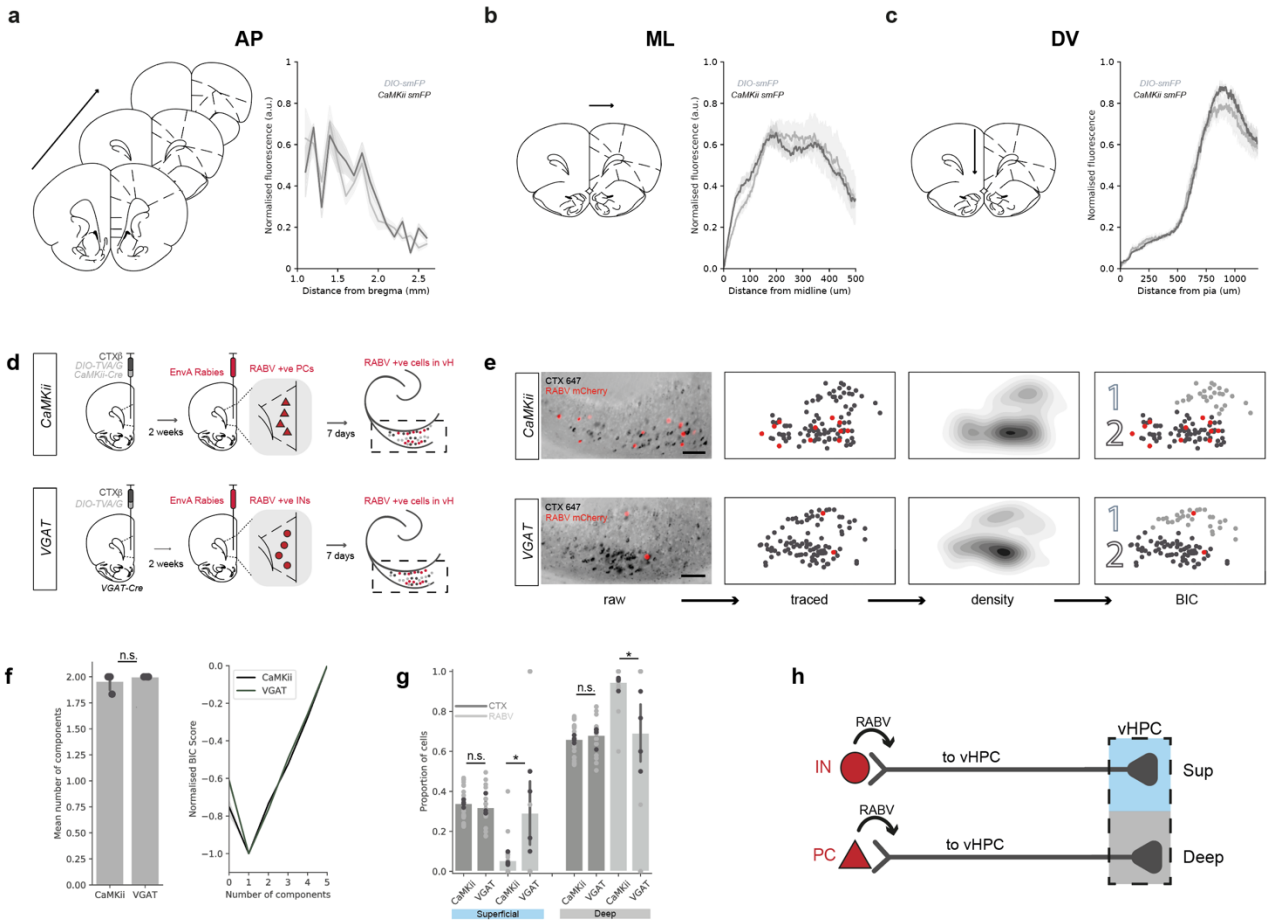

Supplementary Figure 5. Quantification of vH-originating axons in PFC and rabies labelling from PFC

a) Normalised fluorescence of superficial and deep vH axons in prefrontal cortex along the mediolateral (AP) axis. Note similar fluorescence for both *Calb1*$^+$ and *CaMKii*$^+$ axons.

b) Normalised fluorescence of axons in prefrontal cortex along the mediolateral (ML) axis. Note similar fluorescence for both *Calb1*$^+$ and *CaMKii*$^+$ axons.

c) Normalised fluorescence of axons in prefrontal cortex along the dorsoventral (DV) axis, from pia. Fluorescence peaks similar for both conditions, around the PL/IL border.

d) Schematic of viral approach to trace cellular targets of hippocampal inputs to PFC. A mixture of cholera toxin (CTXβ) and rabies helper proteins was injected into the PFC of either *VGAT-Cre* or wild-type mice (which were co-injected with *AAV2/1-CaMKii-Cre*). After two weeks of expression, EnvA pseudotyped rabies was injected into the PFC to allow for specific retrograde tracing to hippocampus via either *VGAT*$^+$ of *CaMKii*$^+$ neurons. One week of rabies expression was allowed, following which horizontal hippocampal sections were cut for visualization of rabies and CTXβ positive cell bodies.

e) Example images of the CA1/subiculum border with rabies (red) and CTXβ (black) positive cells. Note that no red cells are present in the superficial layer in the *CaMKii-Cre* example, while they are evenly spread in *VGAT-Cre* mice (below). Labelled neurons were clustered using a Gaussian Mixture Model and the best fit was chosen using Bayesian Information Criterion (BIC), see methods for detail.

f) Mean number of components (i.e. cell layers/groups) the traced cells were clustered into. *Right:* Normalised BIC scores for 1 to 6 components. For normalisation between 0 and -1, the maximum value was subtracted from the data, which was then divided by the new minimum. The lowest BIC score represents the best fit of components. Note that there is no difference in best fit of components to the data of PFC-projecting cells for *VGAT-Cre* and *CaMKii-Cre* mice.

g) Proportion of cells labelled with CTXβ or rabies in the superficial and deep components (layers) respectively, in the *VGAT* and *CaMKii* scenarios described in (**h**). The proportion of total CTXβ positive cells in the superficial and deep components did not differ between *VGAT* and *CaMKii* experiments. The proportion of rabies positive cells in the superficial component was higher in *VGAT-Cre* mice. Conversely, in the deep component, the proportion of rabies

positive cells was higher in the CaMKii scenario. Dark grey circles show average proportion per injection, light grey circles show raw data from averaged slices per injection.

h) Summary schematic of the viral strategy and outcome. In the *VGAT-Cre* animals (*top*) rabies jumped one synapse from interneurons (IN) and in *CaMKii-Cre* animals (*bottom*), hippocampal inputs were traced from pyramidal cells (PC). Note that rabies positive cells contacting interneurons were found in the superficial layer in greater proportion than in the deep layer. The converse is true for rabies positive cells in the deep layer, where a greater proportion of pyramidal cell-contacting neurons were seen.

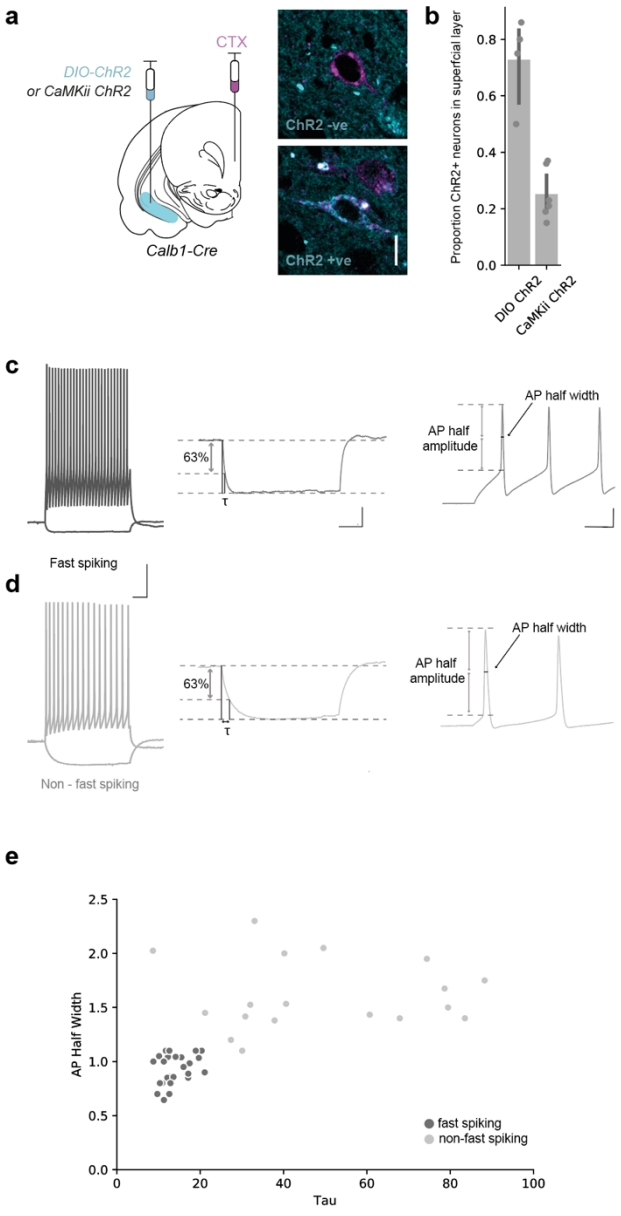

Supplementary Figure 6. Characterization of *Calb1* and *CaMKii* input to PFC and target interneuron subtype

a) *Left,* Schematic summarizing the injections carried out to study vH input to PFC. DIO-*ChR2* or *CaMKii-ChR2* was injected into the vH of *Calb1-Cre* mice two weeks prior to recordings, and CTXβ was injected into PFC to label PFC-projecting vH neurons. Right, Example images of CTXβ +ve neurons (that project to PFC) either negative (top) or positive (bottom) for ChR2. Scale bar = 20 µm.

b) Proportion of ChR2 and CTXβ double positive neurons in the superficial layer of vH in each injection condition. Note that the two conditions preferentially label either the superficial or deep layer.

c) Example current clamp recording from *dlx* +ve interneuron in PFC classified as a fast-spiking interneuron. *Left,* example responses to positive and negative current steps. *Middle and Right,* details of currents showing tau, half amplitude and half width of action potentials. Note fast tau and AP half width. Scale bars = 100 ms, 20 mV; 100 ms 2 mV; 10 ms 20 mV.

d) As in (**c**) but for a neuron classified as a non-fast-spiking interneuron. Note slower tau and bigger AP half width.

e) Clustering of *dlx* +ve interneurons into fast-spiking and non-fast-spiking based on action potential half width and tau. Classifications are used in ***Fig.2.m-p***.

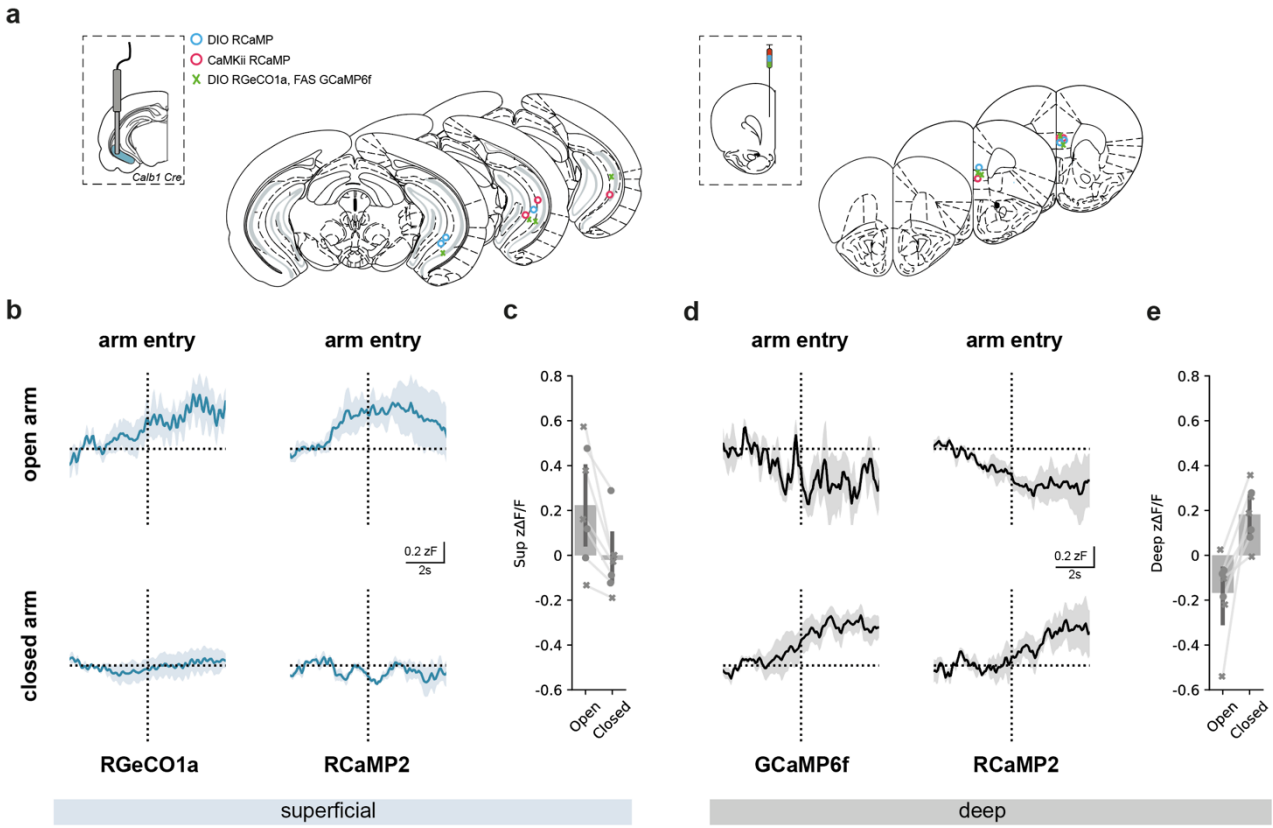

Supplementary Figure 7. Injection site coordinates and sensor specific signals for *in-vivo* calcium imaging

a) *Left* Schematic of fiber photometry implant in vH in a *Calb1-Cre* mouse and histology showing the location of the fiber implants. *Right* Schematic of viral injection into PFC – all viral constructs used for these experiments were retrograde. Each injection and placement is represented as a blue circle for animals injected with DIO RCaMP, red circles for CaMKii RCaMP and green crosses for double-imaging experiments where animals were injected with DIO RGeCO1a and FAS GCaMP6f.

b) Superficial layer neuron calcium fluorescence aligned to open (*top*) and closed (*bottom*) arm entry. Superficial layer neurons seem to respond only to open arm entry. Fluorescence increases upon open arm entry, and remains unchanged on closed arm entry. Note that the activity recorded in these cells does not qualitatively differ based on calcium indicator (RGeCO1a on *left* and RCaMP2 on *right*).

c) Quantification of change in fluorescence from open to closed arm entry. Crosses represent RGeCO1a signal and dots represent RCaMP2 signal.

d) Deep layer neuron calcium fluorescence aligned to open (*top*) and closed (*bottom*) arm entry. Deep layer neurons respond to both open and closed arm entry. Fluorescence decreases upon open arm entry, and increases on closed arm entry. Note that the activity recorded in these cells does not differ based on calcium indicator (GCaMP6f on *left* and RCaMP2 on *right*).

e) Quantification of change in fluorescence from open to closed arm entry. Crosses represent GCaMP6f signal and dots represent RCaMP2 signal.

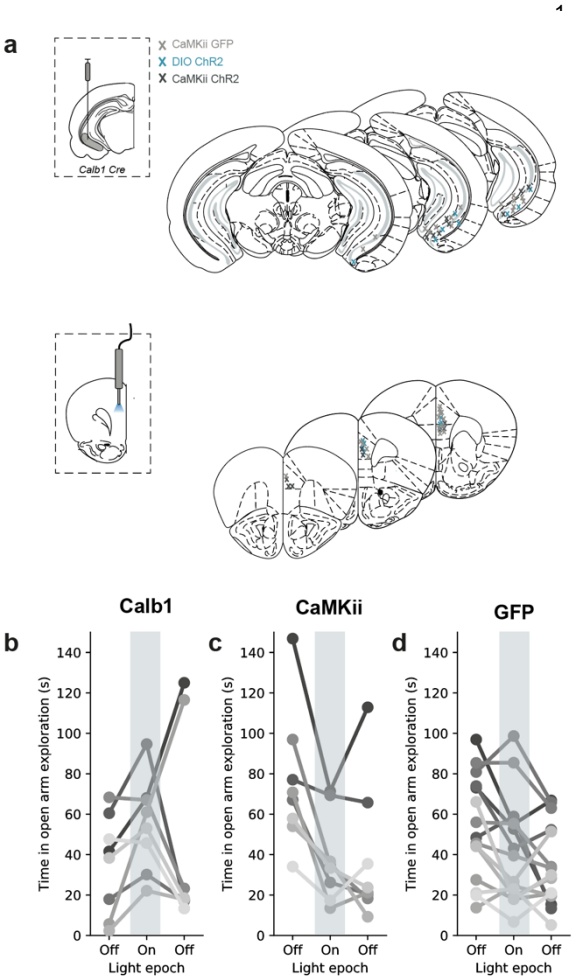

Supplementary Figure 8. Injection site coordinates and raw exploratory behavioral data for *in vivo* optogenetics

a) *Top* Schematic of injection into vH in a *Calb1-Cre* mouse and histology showing the location of injections. *Bottom* Schematic of fiber implant placed over PFC and histology showing fiber placement. Each injection and placement is represented as a blue cross (Calb1 ChR2), dark grey cross (CaMKii ChR2), and light grey cross (CaMKii GFP).

b) Time spent in open arm exploration during three 3-minute epochs (light off, on and off respectively) for *Calb1-Cre* animals injected with DIO-ChR2 in vH and with an optic fiber stimulating axon terminals in PFC. Note that animals engage in higher open arm exploration when the light is on, activating the hippocampal-PFC Calb1 expressing axonal population. Separate traces represent different animals (n = 8).

c) As in **(b)** for animals injected with CaMKii-ChR2 in vH. Note that animals decrease their time spent engaging in open arm exploration when the light is on, activating CaMKii-expressing hippocampal-PFC axons (n = 8),

d) As above, for animals injected with light insensitive CaMKii-GFP in vH. Note that there is no consistent change in behavior from ‘off’ to ‘on’ epochs (n = 15).

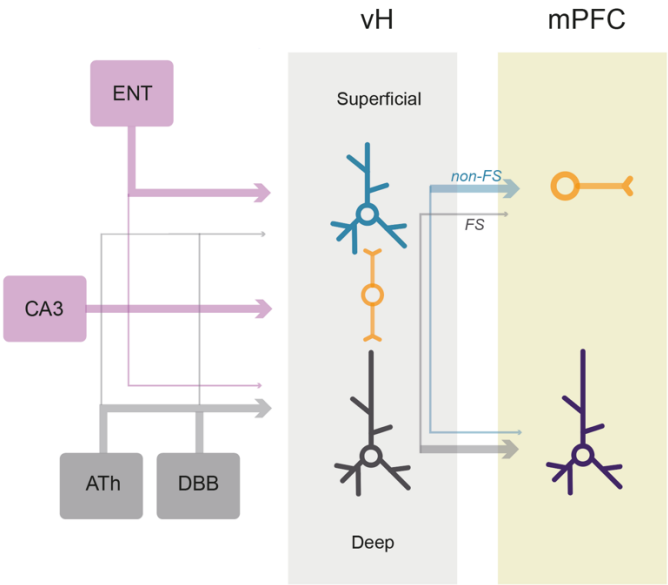

Supplementary Figure 9. Schematic of overall circuit model

In this summary schematic, the main circuit findings are highlighted. In pink (top left), intra-hippocampal inputs to superficial and deep layer PFC-projecting cells. While medial entorhinal cortex (ENT) inputs are biased towards superficial cells, CA3 inputs equally target both layers. In grey (bottom left), long-range inputs to hippocampal PFC-projecting cells from the anterior thalamus (ATh) and the diagonal band of Broca (DBB) bias towards cells in the deep layer. The thickness of the lines represents connection strength. Within the ventral hippocampus (grey box) interneurons (orange) target and are targeted by both superficial (blue) and deep (black) PFC-projecting cells. Superficial cells then go on to preferentially target fast-spiking (FS) and non-fast-spiking (non-FS) interneurons in PFC and deep cells preferentially target pyramidal cells and FS interneurons.

FIGURE	DESCRIPTORS	N	TEST USED	TEST STATISTIC	P VALUE
Sup1g	Superficial: mean +/- sem Deep: mean +/- sem	4 4	Fisher's exact	Odds ratio = 0.0	p = 2.063e-07
Sup1h	Superficial: mean +/- sem Deep: mean +/- sem	12 12	Mann Whitney	U = 0.0	p = 3.658e-05
Sup 2b	Superficial: mean +/- sem Deep: mean +/- sem	22 26	Repeated measures ANOVA with Greenhouse-Geisser correction Interaction of cell type x step	$F_{(1.35,44.48)} = 4.3$	p = 0.032
Sup 2c	Superficial: mean +/- sem Deep: mean +/- sem	22 26	Mann Whitney	U = 393	p = 0.028
Sup 2d	Superficial: mean +/- sem Deep: mean +/- sem	22 26	Mann Whitney	U = 353	p = 0.168
Sup 2e	Superficial: mean +/- sem Deep: mean +/- sem	22 26	Mann Whitney	U = 331.5	p = 0.336
Sup 2f	Superficial: mean +/- sem Deep: mean +/- sem	22 26	Mann Whitney	U = 39.5	p = 0.002
Sup 2g	Superficial: mean +/- sem Deep: mean +/- sem	22 26	Mann Whitney	U = 175	p = 0.034
Sup 2h	Superficial: mean +/- sem Deep: mean +/- sem	22 26	Mann Whitney	U = 139	p = 0.002
Sup 2i	Superficial: mean +/- sem Deep: mean +/- sem	22 26	Mann Whitney	U = 423	p = 0.004
Sup 2j	Superficial: mean +/- sem Deep: mean +/- sem	22 26	Mann Whitney	U = 365	p = 0.104
Sup 2k	Superficial: mean +/- sem Deep: mean +/- sem	22 26	Mann Whitney	U = 166	p = 0.001
Sup 2l	Superficial: mean +/- sem Deep: mean +/- sem	22 26	Fisher's exact test	Odds ratio = 12.5	p = 0.009
Sup 2n	Superficial: mean +/- sem Deep: mean +/- sem	7 6	Mann Whitney	U = 0.0	p = 0.003
Sup 2o	Basal mean dendritic length: Superficial: mean +/- sem Deep: mean +/- sem	7 6	Repeated measures within and between subjects ANOVA with Greenhouse-Geisser correction for sphericity	$F_{(3.337,36.711)} = 1.701$	p = 0.179
Sup 2p	Apical mean dendritic length: Superficial: mean +/- sem Deep: mean +/- sem	7 6	Repeated measures within and between subjects ANOVA	$F_{(35,385)} = 1.549$	p = 0.027
Sup 2s	Nexus: Superficial: mean +/- sem Deep: mean +/- sem	7 6	Mann Whitney	U = 38.5	p = 0.015
Sup 2t	Longest dendrite: Superficial: mean +/- sem Deep: mean +/- sem	7 6	Mann Whitney	U = 35.5	p = 0.045
Sup 2v	Cumulative count by order: Superficial: mean +/- sem Deep: mean +/- sem	7 6	Repeated measures within and between subjects ANOVA with Greenhouse-Geisser	$F_{(5.053,55.694)} = 0.262$	p = 0.934
Sup 2w	Cumulative dendrite length by order: Superficial: mean +/- sem Deep: mean +/- sem	7 6	Repeated measures within and between subjects ANOVA with Greenhouse-Geisser	$F_{(4.715,51.868)} = 0.610$	p = 0.683

FIGURE	DESCRIPTORS	N	TEST USED	TEST STATISTIC	P VALUE
Sup 4i	SC - superficial:deep ratio	10	Wilcoxon paired	V = 33	p = 0.625
	mean+/- sem	10			
Sup 4l	TA- superficial:deep ratio	14	Wilcoxon paired	V = 21	p = 0.049
	mean+/- sem	14			
Sup 5f	CaMKii: mean +/- sem	4	Fisher's Exact	Odds ratio = 0.0	p = 1
	VGAT: mean +/- sem	4			
Sup 5g	Superficial CTX:				
	CaMKii	4	Mann Whitney	U = 12	p = 0.312
	VGAT	4			
	Superficial RABV:				
	CaMKii	4	Mann Whitney	U = 16	p = 0.030
	VGAT	4			
	Deep CTX:				
	CaMKii	4	Mann Whitney	U = 4	p = 0.312
	VGAT	4			
	Deep RABV:				
	CaMKii	4	Mann Whitney	U = 0	p = 0.030
	VGAT	4			
Sup 6b	DIO ChR2	4	Mann Whitney	U = 24	p = 0.014
	CaMKii ChR2	6			

1